Absence of far-red emission band in aggregated core antenna complexes

Ara, Anjue Mane; Ahmed, Mohammad Kawsar; D'Haene, Sandrine; van Roon, Henny; Ilioaia, Cristian; van Grondelle, Rienk; Wahadoszamen, Md

published in
Biophysical Journal
2021

DOI (link to publisher)
10.1016/j.bpj.2021.02.037

document version
Publisher's PDF, also known as Version of record

Biophysical *Journal*
Article

Biophysical Society

Absence of far-red emission band in aggregated core antenna complexes

Anjue Mane Ara,[1,2] Mohammad Kawsar Ahmed,[2] Sandrine D'Haene,[1] Henny van Roon,[1] Cristian Ilioaia,[3] Rienk van Grondelle,[1] and Md. Wahadoszamen[1,4,*]

[1]Biophysics of Photosynthesis, Department of Physics and Astronomy, Faculty of Sciences, VU University Amsterdam, Amsterdam, the Netherlands; [2]Department of Physics, Jagannath University, Dhaka, Bangladesh; [3]Institute for Integrative Biology of the Cell, CEA, CNRS, Université Paris-Saclay, Gif-sur-Yvette, France; and [4]Department of Physics, University of Dhaka, Dhaka, Bangladesh

ABSTRACT Reported herein is a Stark fluorescence spectroscopy study performed on photosystem II core antenna complexes CP43 and CP47 in their native and aggregated states. The systematic mathematical modeling of the Stark fluorescence spectra with the aid of conventional Liptay formalism revealed that induction of aggregation in both the core antenna complexes via detergent removal results in a single quenched species characterized by a remarkably broad and inhomogenously broadened emission lineshape peaking around 700 nm. The quenched species possesses a fairly large magnitude of charge-transfer character. From the analogy with the results from aggregated peripheral antenna complexes, the quenched species is thought to originate from the enhanced chlorophyll-chlorophyll interaction due to aggregation. However, in contrast, aggregation of both core antenna complexes did not produce a far-red emission band at ~730 nm, which was identified in most of the aggregated peripheral antenna complexes. The 730-nm emission band of the aggregated peripheral antenna complexes was attributed to the enhanced chlorophyll-carotenoid (lutein1) interaction in the terminal emitter locus. Therefore, it is very likely that the no occurrence of the far-red band in the aggregated core antenna complexes is directly related to the absence of lutein1 in their structures. The absence of the far-red band also suggests the possibility that aggregation-induced conformational change of the core antenna complexes does not yield a chlorophyll-carotenoid interaction associated energy dissipation channel.

SIGNIFICANCE To cope with the deleterious effects of excess light, photosynthetic organisms developed protective mechanisms that allow the dissipation of the excess energy safely by several physiological mechanisms. Photoinduced rearrangement of protein conformation simultaneously at different sites of photosystem II is one such mechanisms. The peripheral antenna complexes have been considered to be the active sites of conformational rearrangement associated with energy dissipation. The conformational rearrangement of core antenna complexes is also believed to confer essential functions for circumventing the yield of photodegraded photosystem II proteins generated under extreme light stress. This study helps to understand whether and how the aggregation-induced conformational changes of core antenna complexes differ, spectroscopically and in terms of physical properties, from the peripheral antenna complexes.

INTRODUCTION

Photosynthesis is the process of conversion of solar energy into storable chemical energy. In this process, solar photons are absorbed and transferred to photochemical reaction centers (RCs) on an ultrafast timescale and with a very high efficiency (90% or higher). In these special complexes, photochemical charge separation and subsequent secondary transmembrane electron transport take place. To harvest solar energy in a specific spectral window, photosynthetic organisms contain light-harvesting antenna complexes (LHCs) comprising a highly packed and conserved array of chlorophylls (Chls) and carotenoids (Cars) pigments bound to the protein scaffold. Photosystem II (PSII) of green plants contains three types of LHCs: peripheral antenna comprising the major light-harvesting antenna complexes II (LHCII), minor antenna complexes (CP24, CP26, and CP29) and the core antenna complexes (CP43 and CP47) (1). Note that all the LHCs bind different types of Chls and Cars to harvest and process solar energy; each peripheral antenna complex binds two types of Chls (Chl *a* and Chl *b*) and three different types of Cars (luteins, neoxanthin, and xanthophyll cycle carotenoids) (2), whereas both core

Submitted September 11, 2020, and accepted for publication February 22, 2021.

*Correspondence: wahado.phy@du.ac.bd

Editor: Elsa Yan.

https://doi.org/10.1016/j.bpj.2021.02.037

antenna complexes have a single type of Chl (Chl *a*) and Car (β-carotene) (3,4). Elemental events of photosynthesis are predominantly initiated by peripheral antenna complexes, in which both Chls and Cars harvest the available solar photons and subsequently transfer those to the RC for ensuing chemistry (5).

The primary function of the core antenna complexes is to provide an efficient conduit for shuttling solar photons absorbed by the peripheral antenna complexes to the RC of PSII (6). In addition, they fulfill a number of vital functions in the photosynthetic machinery. As active light harvesters, they also absorb light energy (via Chl *a* and β-carotene cofactors) and subsequently transfer the energy to the RC (7). They have some structural functions as well; they stabilize the oxygen-evolving site (8–11), provide a binding site for the Mn-stabilizing 33-kDa protein (12), and facilitate the light-induced formation of a tyrosine radical in the reaction center (13). The two Chl-binding proteins CP43 and CP47 are structurally similar and thought to have evolved from a common ancestor (14); however, several differences were found, including in their spectroscopic properties (15) and structural and functional roles in PSII (7).

Although light is the most essential ingredient of the photosynthetic reaction, when in excess, this can be harmful to the photosynthetic machinery (16). An excess amount of light harvested by photosynthetic antenna pigments is believed to assist the formation of highly toxic chemical byproducts that can potentially damage (photodamage) the photosynthetic apparatus.

Photosynthetic organisms have the inbuilt ability to avoid deleterious effects of excess sunlight by employing a series of strategies (5,17–23). Change of protein conformation occurring/exiting on a timescale of minutes simultaneously at different sites of PSII is one such protocols (18,22,24–26). It is suggested that conformational change of protein can modulate delicately pigment-pigment and/or pigment-protein interactions (22,24,25,27), induce aggregation and/or cross-linking (19,20,28), and thereby open up pathways to dissipate excess absorbed excitation energy or dictate the pertinent pigment-protein complexes to trigger necessary protective functions. To this end, conformational change of peripheral antenna complexes is believed to play a central role in dissipating the excess absorbed excitation energy before it assists the formation of toxic byproducts (22,24,25). The conformational change of core antenna complexes, on the other hand, are believed to confer essential functions, by themselves or in association with other neighboring polypeptides, to diminish the yield of photodegraded proteins generated under extreme light stress (19,20). It is also predicted in some studies that, like peripheral antenna complexes, the core antenna complexes may also participate in photoprotective excitation energy quenching (29,30).

Artificial aggregation upon detergent removal is considered to be a simple but efficient means to induce conformational change to light-harvesting antennas of photosynthetic organisms; thus, it is often regarded to be a model method to mimic photoprotective energy dissipation brought about via excess light-induced conformational change (5,22,24,25). The artificially aggregated major antenna complex (LHCII) was first used in the early 1990s to mimic conformational change-induced excess energy dissipation in vivo (31). From the observed drastic modification of spectroscopic behavior and remarkably low light-harvesting efficiency, it was hypothesized that aggregation of LHCII leads to the prompt dissipation of absorbed energy into heat. Similar spectroscopic features were found when the aggregated complexes were compared with energy dissipation in vivo (32,33). Recently, by using series of freeze-fracture electron microscopy studies, it was shown that LHCII antenna aggregation takes place in vivo when excess energy dissipation is established (26). This technique, combined with computer image analysis, established that, in the energy-dissipating state, the intertrimer distances became shorter, implying the formation of protein clusters resembling the LHCII aggregates in vitro (26).

To characterize aggregated photosynthetic pigment-protein complexes with a view to better understand the conformational change-induced energy dissipation mechanism, over the last couple of years, we have been applying Stark fluorescence (SF) spectroscopy to the native and aggregated peripheral antenna complexes of different organisms (34–37). The systematic and comprehensive analyses of SF spectra revealed that the aggregation of all of these pigment-protein complexes results in the formation of multiple spectrally overlapping emissive species. Among them, an emissive species giving a very broad emission at around 700 nm was present ubiquitously in all the aggregated antenna complexes (34–36). From the magnitude of the physical parameters estimated from the analyses of SF spectra, we ascribed the 700-nm broad emission band to arise from the enhanced Chl-Chl interaction, in agreement with other reports present in the literature (38,39). In addition, an emissive species displaying an emission feature with very weak intensity (relative to the 700-nm band) in the 720- to 740-nm spectral region was found to be common in the dissipative states of most of the antenna complexes. From its very feeble intensity and extraordinarily large electric field effect, we hypothesized that the far-red species is generated mainly from the enhanced Chl-Car interaction arising from the aggregation-induced conformation change in and around the terminal emitter domain (34–37). Comprehensive and systematic analyses of the SF spectra uncovered the exceptionally large magnitude of the charge-transfer (*CT*) character of the far-red species, which further strengthens our proposition that Car is involved in its formation.

Under extreme light stress, when unwanted photoinhibition of PSII tends to be predominant, different core antenna proteins undergo rapid turnover. One of the mechanisms by

which such a turnover was found to occur, both in vivo and in vitro, is the photoinduced noncovalent aggregation of different core antenna proteins with RC-binding D1 protein (20). It has been hypothesized that such aggregated adducts are produced mostly by the local change in protein conformation, which eventually imposes a strong barrier to the conversion of PSII proteins to photodamaged products. It was also observed that high light-induced protein oxidation triggers aggregation to core antenna proteins as one of the protective strategies (19). Because it is supposed to be activated by the local change of protein conformation, one can expect that the aggregation event of the two pigment-binding core antenna proteins (CP43 and CP47) would be accompanied by tangible modifications on their pigment-pigment and/or pigment-protein interactions. If it were, the aggregated pigment-binding core antenna proteins would give very different spectroscopic signatures as compared with their native proteins. However, detailed knowledge about the spectroscopic nature and the underlying physical properties of the aggregated pigment-binding core antenna protein is lacking so far. To uncover the spectroscopic and physical properties, we have applied SF spectroscopy on both aggregated and native CP43 and CP47 core complexes. Aggregated CP43 and CP47 complexes were obtained by removing the detergent from their isolated proteins. The key motivation of this work stemmed from the simple assumption that, like for peripheral antenna complexes, the aggregated core antenna complexes display some emission species different from the ones of their isolated forms. In this case, SF spectroscopy is the suited experimental tool for unraveling their physical properties and hence offers the unique opportunity to make a qualitative comparison with the SF results obtained for peripheral antenna complexes (34,35). Such comparison would help one to understand how the energy dissipation induced by the alteration of pigment-pigment interaction upon aggregation in core antenna complexes differs from the peripheral antenna complexes. Additionally, the spectroscopic characterization of the aggregated pigment-binding core antenna proteins would also provide insights into how pigment-pigment interaction in core antenna proteins is modulated.

MATERIALS AND METHODS

Isolation of PSII core antenna complexes

Core antenna CP43 and CP47 were prepared from PSII core complexes from spinach, as described by Ghanothakis et al. (40), which were solubilized with n-dodecyl-β,D-maltoside (β-DM) and purified by ion exchange chromatography, according to the protocol of Dekker et al. (41) with modifications as in Groot et al. (42) for CP43 and as in Groot et al. (43) for CP47.

Pigment analysis

Total pigments were extracted in 80% ice-cold acetone and centrifuged for 5 min at maximal speed on a bench centrifuge. Total Chl concentration and Chl *a*/*b* ratios were calculated using the extinction coefficient of Porra et al. (44) from absorption at 750, 663.6, and 646.6 nm. Xanthophyll composition was determined by reversed-phase high-performance liquid chromatography according to the method of Gilmore et al. (45). Resolution of lutein and zeaxanthin was achieved using a non-endcapped, lightly carbon-loaded C18 high-performance liquid-chromatographic column (45) using a Li-Chrosorb C18, 10-μm, 250 $\times$ 4.6-mm column connected with an on-line diode array detector (SPD-M10Avp; Shimadzu, Kyoto, Japan), which allows pigment identification and quantification by the absorption spectra.

Stark spectroscopy

The aggregated CP43/CP47 sample was obtained by incubation of the isolated detergent-containing complex with 50 mg of SM-2 Absorbent (Bio-Rad Laboratories, Hercules CA), allowing a 10-fold decrease of the fluorescence (F) intensity (i.e., the F intensity was reduced by ~90%). Native CP43/CP47 was prepared by suspending the isolated core complexes in a buffer containing 20 mM Hepes (pH-7.5), 20 mM NaCl, 10 mM $MgCl_2$, and 0.06% β-DM. The CP43/CP47 sample was then diluted with 60% (v/v) glycerol for producing a transparent glass at 77 K. The aggregated CP43/CP47 was similarly prepared, except the buffer contained no detergent (e.g., β-DM). SF spectroscopy was performed on the transparent frozen glasses of native and aggregated antennas at 77 K in a cell prepared by gluing two quartz slides, having inner surfaces coated with thin transparent layers of indium tin oxide, with double-sided sticky tape (Sellotape, Winsford, UK). The optical path length of the constructed cell was estimated by comparing absorption spectra of the sample measured through the cell and through a cell of known path length of 1 mm to be 100 μm with standard error of ± 3 μm. The SF experiment was carried out on a custom-built setup, as described previously (34–37,46–48). In this setup, the light of a Xenon lamp (Oriel, Newport, UK) is passed through a monochromator (1200 gmm^{-1} grating blazed at 350 nm) for producing the desired excitation wavelength. The excitation beam, after being horizontally polarized through a Glan-Taylor Polarizer, impinges on the Stark cell containing the sample under an angle of 45°. The Stark cell is immersed into the liquid N2 chamber of an Oxford cryostat (DN1704; Oxford Instruments, Abingdon, UK) which has strain-free transparent quartz optical windows. A sinusoidal AC voltage of minimal distortion synthesized in the lock-in amplifier (SR850) with a modulation frequency of ω (=80 Hz) was applied to the sample after desired amplification through a high-voltage generator. Both the F and SF signals were, after being detected by a photomultiplier tube, recorded simultaneously by the lock-in amplifier at the second harmonics 2ω of the modulation frequency. The details about the theoretical modeling of experimentally obtained SF data can be found elsewhere in the literature (34,48–52). Briefly, the SF spectrum of homogeneously distributed and spatially fixed chromophores in a solid matrix (having negligible interchromophore interaction) can fairly be approximated as the weighted superposition of the zeroth-, first-, and second-order derivatives of the (field-free) F spectrum expressed by the following equation:

$$\frac{2\sqrt{2}\Delta F(\nu)}{F_{\max}} = (fF_{ext})^2\left\{A_\chi F(\nu) + B_\chi \nu^3 \frac{d[F(\nu)/\nu^3]}{d\nu} + C_\chi \nu^3 \frac{d^2[F(\nu)/\nu^3]}{d\nu^2}\right\}, \quad (1)$$

where F_{max} is the F intensity at the maximum, F_{ext} is the magnitude of the electric field applied externally during the course of experiment, ν is the energy in wavenumber, χ is the experimental angle between the direction of F_{ext} and the electric vector of the excitation light, and f is the local field correction factor used to estimate the magnitude of the internal electric field experienced by the chromophore(s), F_{int} via the relation $F_{int} = fF_{ext}$. The coefficient A_χ (denoted hereafter as zeroth derivative contribution (*ZDC*))

reflects the field-induced change in emission intensity arising mostly from field-induced modulation of the rates of nonradiative deactivations competing with the F process (48,49,53). In addition, the coefficients B_χ and C_χ are associated with the electro-optic parameters, more specifically, changes in molecular polarizability ($\Delta\alpha$) and molecular dipole moment ($\Delta\mu$) between the ground and excited states connected by the optical transition, respectively (48,49,53). At the magic angle ($\chi = 54.7°$) the mathematical expressions of B_χ and C_χ are greatly simplified and can be expressed as:

$$B_{54.7°} = \frac{\Delta\alpha}{2hc} \tag{2}$$

and

$$C_{54.7°} = \frac{(\Delta\mu)^2}{6h^2c^2}. \tag{3}$$

Therefore, upon reproducing the SF spectrum by a weighted superposition of the derivatives of the corresponding F spectrum and computing the coefficients of the first- and second-order derivatives, one can extract the values of $\Delta\alpha$ and $\Delta\mu$ from the above two equations. Because the value of the local field correction f is not known, the values of $\Delta\alpha$ and $\Delta\mu$ in this study are expressed in terms of f. All the SF spectral fitting protocols of this study were performed using the commercially available Igor (WaveMetrics, Portland, OR) software routine.

RESULTS

Fig. 1 displays F (*top*) and SF (*bottom*) spectra of native and aggregated CP43 (*left*) and CP47 (*right*). Here and hereafter, the native/aggregated samples of CP43 and CP47 are denoted, respectively, as NCP43/ACP43 and NCP47/ACP47. Both F and SF spectra are recorded simultaneously with excitation at 444 nm for CP43 and 443 nm for CP47, where,

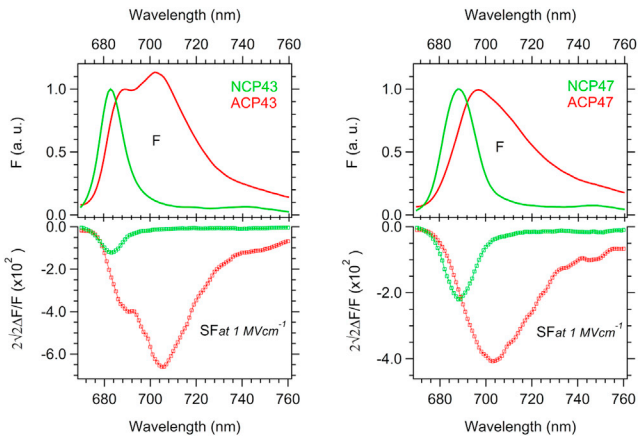

FIGURE 1 F (*top*) and SF (*bottom*) spectra of native (*green curves*) and 10-fold aggregated (*red curves*) CP43 (*left panel*) and CP47 (*right panel*) measured simultaneously at 77 K with excitation wavelengths of 444 and 443 nm, respectively. The F spectra are normalized to unity at their peaks, whereas the SF spectra are normalized to the intensity of the corresponding F peaks and to the field strength of 1 MVcm^{-1}. For all the complexes, the SF spectrum is seemingly identical in shape to the respective F spectrum, demonstrating that the SF spectrum has a significant zeroth-order derivative (of the F spectrum) contribution. To see this figure in color, go online.

because of overlapping contributions of Stark absorption (SA) signals that cancel each other, the net electric field-induced change in extinction is negligible (see Fig. S1). Among the several zero-crossings available in the SA spectrum, we used the zero-crossing wavelength 444/443-nm as the excitation wavelength for SF measurements of CP43/CP47 because the wavelength resides around its (CP43/CP47) blue absorption maximum peaking around 438 nm (see Fig. S1). This was done to record the optimum F intensity and, hence, the better signal-to-noise (*S*/*N*) ratio in SF measurement. In fact, both F and SF spectra for each sample were measured at different field strengths within the range 0.3–0.5 MVcm^{-1}, then the average SF signal was calculated upon normalizing the SF spectra to the field strength of 1 MVcm^{-1} and to the peak intensity of the F spectrum. This type of SF protocol offers one the unique opportunity to check the quadratic field dependence of the SF signal and thereby, at the same time, to have better *S*/*N* upon averaging. Note that the coefficient of the zeroth-order derivative (of F spectrum) was found to be negligibly affected by such normalization protocol. The F spectra of native CP43 and CP47 show a sharp excitonic band of Chl *a* with a peak at around 683 and 688 nm, respectively. Both F spectra are accompanied by a broad vibrational satellite, with very weak intensity peaking at around 742 nm in CP43 and 747 nm in CP47. The characteristic sharp excitonic band of Chl *a* with vibrational tail is a typical emission feature observed in the light-harvesting state in all native photosynthetic pigment-protein complexes of photosynthetic organisms (33–35,54). The F spectrum of both aggregated complexes is apparently a juxtaposition of two bands. For ACP43, the two bands are clearly resolved and peak at 688 and 702 nm. The 688-nm band is, to some extent, sharp and structurally resembles the excitonic emission lineshape of the native CP43 available in the aggregated sample. On the other hand, 702 nm is characterized by a strikingly broader lineshape, with a long tail extending up to the end of the spectral window. The broader 702-nm band gives a dominant appearance in the overall emission spectrum and is considered to be the emission signature of the quenched species. The F spectrum of ACP47 is also characterized by the presence of two closely lying bands; however, in this case, the overall shape of the spectrum is dominated by the excitonic-like emission lineshape (with a peak at 697 nm), whose red tail is adorned with the shallow presence of a broader emission lineshape (with a peak at around 705 nm) of the quenched species. Note that such a broad and diffused fluorescence spectral feature was found to be common to almost all aggregated antenna complexes and is thus considered as the spectral signatures of some quenching species (34–36,38).

Both aggregated and native CP43 and CP47 yielded SF spectra characterized by negative amplitudes with shapes merely identical to the corresponding F spectra. However, the SF amplitudes of aggregated and native samples are

found to be notably different. ACP43 and ACP47 complexes yielded ∼six- and ∼four-fold more negative SF intensity compared with their native counterparts, respectively. Similar field-induced spectroscopic features were also observed for all the (native and aggregated) antenna complexes studied so far with SF spectroscopy (34–36). The broad negative SF bands of ACP43 and ACP47 peak at 705 and 702 nm, respectively, which are 3 and 5 nm red shifted with respect to the peaks of the corresponding F bands. The overall large negative amplitudes, together with the larger red-shifted peaks, indicate that the observed SF lineshapes of aggregated complexes received fairly large contributions from both electric field-induced reduction of F yield and field-induced spectral shift.

SF analysis

Standard Liptay formalism is the mathematical basis routinely used to analyze the SF spectra of photoactive chromophores, including the ones of photosynthetic pigment-protein complexes (34,36,46–48,55). The standard Liptay formalism-associated protocol is the simplest approach toward analyzing Stark results of photosynthetic pigment-protein complexes, which is guided by an assumption that there exists negligible excitonic interaction among the emitting pigments, although in reality, tangible intrapigments excitonic interaction is believed to be the common incidence for such complexes (54,56,57). Despite this, the standard Liptay formalism has been proven to be a suitable mathematical tool for producing acceptable modeling of SF spectra of a variety of (both native and aggregated) photosynthetic antenna complexes (34–36,46,47).

According to the Liptay formalism, if the F (and hence the SF) signal around a certain wavelength window is originated from a single type of noninteracting emissive species, the weighted sum of the derivatives of the F spectrum can yield a plausible and realistic fit of the SF spectrum. However, this theoretical prescription does not apply when both signals originate from multiple distinct spectral species. Owing to their intrinsic different physical origin, the multiple species may have distinct electrostatic properties and, hence, exhibit different responses to the electric field and yield different amplitudes and shapes of the SF signals. In such a case, the linear superposition of the derivatives of the observed F spectrum cannot synthesize a plausible fit of the SF spectrum throughout the wavelength window but often yields a nonnegligible margin of disagreement in some wavelength regions (34–36,46,47). To circumvent such pitfalls, the observed F spectrum needs to be deconvoluted into a set of bands representing the emission signatures of the available multiple species. The weighted sum of the derivatives of the deconvoluted bands can then be used to obtain a satisfactory fit of the SF spectrum.

The SF spectrum of both native antenna complexes could be well reproduced by the weighted superposition of the derivatives of the corresponding (field-free) F spectrum without deconvolution with a dominant contribution of the (negative) zeroth-order derivative and negligible contributions of first- and second-order derivatives (Fig. 2). This is expected because the shapes of the SF spectra are virtually identical to the shapes of the corresponding F spectra, and here, we found only weak field-induced peak shifts and modification of bandwidths and no field-induced distortion in the band shapes. Altogether, these findings suggest that, as with other native photosynthetic antenna complexes, the F spectra of each native complex originate from a single excited electronic state that corresponds to the lowest exciton state. The satisfactory fit of the SF spectrum by a weighted superposition of the derivatives of the observed F spectrum further substantiates the fact that, albeit implemented with the assumption that there exists non-negligible intrapigment interaction, the standard Liptay formalism is capable enough to produce realistic modeling of the Stark results of photosynthetic pigment-protein complexes.

On the other hand, the failure to reproduce the SF spectrum for both ACP43 and ACP47 by a weighted superposition of the derivatives of the corresponding field-free F spectra without deconvolution has provided us with the rational ground to perform deconvolution-associated modeling (data not shown). We then attempted to model the F spectrum of ACP43/ACP47 upon deconvoluting its F spectrum into three constituent bands denoted as b1/b′1, b2/b′2, and b3/b′3 (Fig. 3, *left*/*right panel*). In this protocol, the b1/b′1 band, a single symmetric Gaussian with peak at 670 nm, is necessary to address the F signal around the shorter wavelength tail and considered to be the spectral signature of free Chls present in the ACP43/ACP47 preparation. Some free Chls are often present both in aggregated

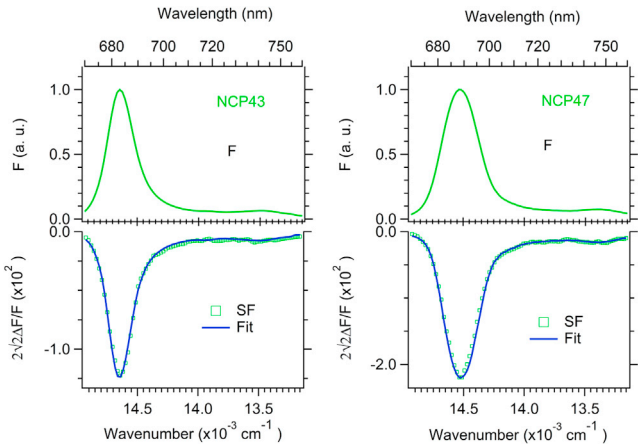

FIGURE 2 F spectrum (*green solid line*, *top*), SF spectrum (*green dotted line*, *bottom*), and the fit of SF spectrum (*blue solid line*) of NCP43 (*left panel*) and NCP47 (*right panel*). The fit of the SF spectrum was obtained by the weighted superposition of the zeroth-, first-, and second-order derivatives of the F spectrum without deconvolution. To see this figure in color, go online.

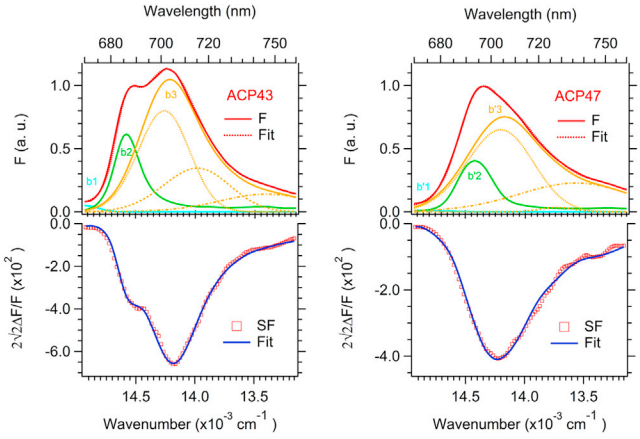

FIGURE 3 (*Top*) F spectrum (*red solid line*) of ACP43 (*left panel*)/ACP47 (*right panel*) and the corresponding fit (*red dashed line*) obtained with a linear combination of a supposed emission lineshape of free Chls, an excitonic-like band (produced by 3/5-nm red shifting of the F lineshape of native CP43/CP47), and a broad inhomogeneously broadened lineshape synthesized by a linear combination of 3/3 symmetric Gaussian functions shown by three broken lines within its envelope. (*Bottom*) SF spectrum and the corresponding fit (*blue solid line*) obtained with the weighted superposition of the zeroth-, first-, and second-order derivatives of the deconvoluted bands. To see this figure in color, go online.

and native photosynthetic antenna complexes, and it is assumed that they neither involve in excitonic interactions nor have a significant effect on the overall physical properties (42,58). It is impossible, however, to estimate the exact number of such Chls belonging to this group. The b2/b′2 is the weighted contribution of the 3/5-nm red-shifted native CP43/CP47 F lineshape and is considered as the contribution of the excitonic emission of bound Chl *a*. The use of the shape of the emission of the native CP43/CP47 in the deconvolution protocol is guided by the assumption that the aggregated CP43/CP47 still has some considerable amount of the native complex. To this end, from its rather sharp and structured appearance in the emission spectrum of the aggregated complex (ACP43/ACP47), we assumed that, despite residing in a somewhat conformationally distorted environment, the unaggregated CP43/CP47 fraction retains the emission shape identical to that of native CP43/CP47. In such a line of thinking, the use of the emission lineshape of the native CP43/CP47 in the deconvolution protocol helped us to produce both the sharp excitonic band and the vibrational satellite of the emission of the unaggregated fraction with a fairly small margin of ambiguity. On the other hand, the b3/b′3 band, which peaks at 704/706 nm, is considerably broad and structureless and was synthesized by a linear combination of three/three symmetric Gaussians of varying widths and is considered as the spectral signature of the quenched species in ACP43/ACP47. The SF spectrum of ACP43/ACP47 could then be fairly well reproduced by the linear superposition of the zeroth-, first-, and second-order derivatives of the three deconvoluted bands. Because free Chls have no significant effects on the overall physical properties and are not of interest here, we will not discuss the fitting results of free Chls.

Table 1 compiles the values of the molecular parameters extracted from the SF analyses. In native CP43/CP47, the analysis yields negative *ZDC* (−0.012/−0.021 at a field strength of 1 MV cm^{-1}) and negligible $\Delta\alpha$- and $\Delta\mu$-values. As expected, the obtained negligible magnitude of $\Delta\mu$ indicates that the F state of both native antennas is characterized by negligible *CT* character, and the moderate magnitude of negative *ZDC* indicates that the rates of nonradiative deactivation associated with this state are moderately accelerated by the applied external electric field. For a photoactive chromophore under SF investigation, negative *ZDC* can result from electric field-induced acceleration of the rates of different nonradiative deactivations (such as internal conversion, intersystem crossing, excited-state isomerization, and deactivation to *CT* state etc.) competing simultaneously with its F transition. However, the rates of the most of the nonradiative deactivations, except deactivation to *CT* state(s), were found to be weakly affected by the external electric field (53,59). Therefore, the observed moderate magnitude of negative *ZDC* of native CP43/CP47 is likely to result largely from electric field-induced acceleration of the rates of nonradiative deactivation to nearby *CT* state. If a *CT* state lies in the close neighborhood of an F state, it is quite reasonable to expect that an external electric field greatly enhances the rates of the nonradiative decay to this state.

From the results presented in the table, we can also notice that, for the unaggregated excitonic-like band b2/b′2, the SF analysis yielded a slightly more negative value of $\Delta\alpha$ (−17.9/−35.79 [Å^3/f^2]), almost the same values of $\Delta\mu$, and a five times larger/two times-smaller value of ZDC (−0.050/−0.01 at a field strength of 1 MV cm^{-1}) compared with the excitonic band of native CP43/CP47 (Table 1). The obtained variation in the magnitudes of $\Delta\alpha$ and *ZDC* are likely to result from the fact that the excitonically coupled unaggregated Chls fraction is nestled in a somewhat altered protein microenvironment in aggregated complexes. On the other hand, the identical $\Delta\mu$-values indicate that the modified protein microenvironment does not induce measurable modification on the *CT* character of the excitonically coupled bound Chls.

TABLE 1 Estimated molecular parameters within 10% of standard deviation

Sample	Band	λ_{max} (nm)	*ZDC**(at 1 MVcm^{-1})	$\Delta\alpha$[Å^3/f^2]	$\Delta\mu$[D/*f*]
NCP43	Single	683	−0.012	3.58	0.46
ACP43	b2	686	−0.050	−17.90	0.46
	b3	704	−0.050	−143.17	3.09
NCP47	single	688	−0.021	−3.58	0.46
ACP47	b′2	693	−0.010	−35.79	0.65
	b′3	706	−0.046	17.90	3.09

*zeroth derivative contribution.

In the case of the third band, b3/b′3, our analysis yielded the same magnitude of the *ZDC* (−0.050/−0.046 at the field strength of 1 MV cm^{-1}) for both complexes but yielded significant variation in the magnitudes of $\Delta\alpha$ (−143.17/17.9 [$Å^3/f^2$]). Interestingly, the analysis shows a markedly large magnitude of $\Delta\mu$ (3.09/3.09 [D/*f*]) for this band, which is almost five to seven times larger than the one of b2/b′2 band, even larger than those obtained for analogous bands of the aggregated peripheral (major and minor) antenna complexes (34,35). This indicates that relaxed F states associated with these bands possess considerably large magnitude of *CT* character.

DISCUSSION

For photoactive pigments embedded in membrane proteins, fluorescence spectra often provide a sensitive means of characterizing the conformation and function of proteins. CP43 and CP47 are two types of pigment-binding membrane proteins, which after selective excitation can give a number of fluorescence signals, including fluorescence of aromatic amino acids and pigments (60). To this end, upon UV excitation (at 280 nm), the emission spectra of CP43 and CP47 mainly reflect the presence of aromatic the amino acids tryptophan and tyrosine (61), and the emission is known as UV emission of CP43 and CP47. On the other hand, upon excitation around 430- and 480-nm, the emission spectra of CP43 and CP47 show the characteristic excitonic emission of Chl *a* (62,63), for which cases 430- and 480-nm radiation is absorbed mostly by β-carotene and subsequently transferred to the Chl *a* to produce the F signal. In our present work, we use the excitonic emission of Chl *a* upon excitation at 444- and 443-nm of native CP43 and CP47 antennas, respectively, where the available carotenoid (β-carotene) absorbs. This indicates that the photon energy absorbed by β-carotene could be effectively transferred to Chl *a*, and the integrity of the CP43 and CP47 preparation is maintained to facilitate this energy transfer.

To better understand the molecular mechanism(s) of energy dissipation, over last few years, we have been applying SF spectroscopy to the aggregated states of different antenna complexes of higher plants (i.e., LHCII, CP24, CP26, and CP29), diatoms (FCP, fucoxanthin chlorophyll a/c binding protein), and the cyanobacterial iron stress-inducible pigment-protein complex IsiA (34–37). A common phenomenon that was often observed in these antennas (especially of higher plants and diatoms) is that induction of aggregation via detergent removal always results in a significantly broadened F spectrum, which often contains the signature of the lowest excitonic band of bound Chls as well. From the systematic and comprehensive analyses of SF spectra, we revealed the spectral signature of two distinct emitting pigment species associated with the aggregated states. Of the two emissive species, the first one was clearly resolved and characterized with remarkably broadened lineshape with a peak ∼700 nm. Considering it as a potential candidate for the regulative energy dissipation and, hence, to plausibly infer its molecular identity, the ∼700-nm F state of aggregated peripheral antenna complexes has been studied extensively over the past few decades (25,38,39,64–66). Based on its observation through single-molecule spectroscopy in native LHCII complex and in the arrangements that prevent LHCII aggregation, it has also been proposed that the F state corresponding to ∼700-nm F is an intrinsic feature of LHCII trimer (25,66,67). In keeping with a good analogy with most of the previous studies (38,39,64,65,67), we attributed the ∼700-nm F lineshape of aggregated peripheral antenna complexes to origination from enhanced Chl-Chl interactions due to conformational modulation. From the pronounced broadening, large stokes shift, very small hole-burning efficiency around the 700-nm region (68) and the requirement of the presence of special state in explaining red-shifted single-molecule spectrum (69), it has been proposed that the emitting state of the ∼700-nm F is a *CT* state with strong excitonic character. From the detailed analysis of time-resolved F spectra and quantum chemical computation, the emitting state of the ∼700-nm F has been hypothesized to be a Chl-Chl *CT* state that lies energetically in the close vicinity of Chl-Chl exciton state and, hence, is capable of borrowing a significant amount of F from it to produce a well-defined emission feature (64). Our SF analysis yielded a smaller magnitude of $\Delta\mu$ (within 1 to 2.5 [D/*f*]) for this band, indicating that the corresponding F state possesses rather weak *CT* character. The revealed smaller *CT* character, in fact, substantiates well the assignment that the emitting state of ∼700-nm F is originated from Chl-Chl interaction. If it were generated from Chl-Car interaction, one would expect a larger magnitude of *CT* character of the resulting emitting state because Car has a strong intramolecular *CT* state in its excited manifold mixed with the S1 state (70).

On the other hand, the second F band is a spectrally very weak far-red band peaking at around 730 nm (34–36). The contribution of such a far-red band was also found in the SF spectrum of IsiA of cyanobacteria (37). From its very weak emission feature, coupled with the remarkable response to the electric field and exceptionally large magnitude of $\Delta\mu$-value, we hypothesized that Chl-Car interaction is involved in the formation of the far-red emission band (34–36), although some studies proposed a different origin (38,64). To this end, for the aggregated LHCII, FCP, and cyanobacterial IsiA, the far-red band was assumed to originate from the enhanced interaction of Chls with the carotenoid lutein 1, fucoxanthin, and echinenone, respectively, in the terminal emitter locus. Because the minor antenna complexes (CP24, CP26, and CP29) display a very good sequence homology with major antenna complexes LHCII, we proposed a similar origin for far-red bands observed in their aggregated states (34). Therefore, like for the 700-nm emission bands of the aggregated major and minor antenna complexes, we can attribute the broader emission

band b2/b′2 of the aggregated CP43/CP47 to originate predominantly from the Chl-Chl interaction at the terminal emitter locus. However, the SF analysis of this band yielded a larger magnitude of $\Delta\mu$ compared with the analogous bands of (aggregated) major and minor antenna complexes, indicating that the F state of the aggregated species has larger *CT* character.

The marked difference in magnitude of the *CT* character may result from the different protein microenvironments and conformation of the core antenna complexes that confer favorable position, vicinity, and orientation of Chls for inducing a larger magnitude of intra-Chls interaction after aggregation and, hence, the larger extent of charge dislocation in the resulting aggregated species. Obviously, the molecular structure of Chl *a* is not changed because of aggregation; however, the distance and orientation of the pigments may be tuned as a consequence of the structural modification of protein (6,71). Core antenna complexes are different from the peripheral ones in terms of the amount of lipid, number and type of pigments, and membrane structure. In particular, the extramembrane domains of CP43 and CP47 possesses a certain degree of secondary and tertiary structure (not a complete random coil conformation) and it has been found that the changes in energy transfer from β-carotene to Chl *a* is directly related to the changes in the tertiary structure of protein (63). CP47 protein binds a total of 16 Chl *a* molecules, whereas CP43 protein binds a total of 13 Chl *a* molecules. Under the pseudo-C2 symmetry of the PSII core complex, 13 of the 16 Chls of CP47 have a symmetry partner in CP43. The three additional pigments of CP47, Chls 612(11), 613(12), and 617(16), which have no analog in CP43, lie in the main luminal domain (4). Each Chl molecule is located in a unique binding site in its protein, and the pigment-protein interactions at these binding sites dictate the transition energy or site energy of each pigment (4). Therefore, the integrity in structure, pigmentation, and interior polarity (that depends on the amount of lipid) may lead the core antenna complexes to produce, upon aggregation, very distinct spectral species characterized by a larger magnitude of *CT* character.

Both core antenna complexes are characterized with distinct lowest-energy states (the terminal emitters). To this end, Chls 634(43), 636(45), and 631(37) have been commonly assigned as the three low-energy pigments available in CP43 (30,72). The two among the three suggested low-energy pigments, Chls 634(43) and 636(45), are embedded within large exciton domains, each consisting of six strongly coupled Chls (30). The Chl 631(37) is a bit isolated and forms a dimeric exciton domain with Chl 629(34) (see Fig. 4). From the theoretical modeling of different experimental data, either Chl 634(43) or Chl 636(45) has been assigned as the most probable candidate for the lowest-energy pigment in CP43 (29,74). In contrast, definitive identification of the low-energy pigment of CP47 is complicated and still remains elusive. Yet, Chls 612(11), 622(24), 624(26), and 627(29) have been suggested to be the possible low-energy pigments in CP47 (30,75). The Chls 612(11), 622(24), and 624(26) are parts of large domains, each consisting of seven strongly interacting Chls, whereas Chl 627(29) resides in the peripheral location and forms a very weakly coupled localized exciton domain with the limited number of Chls available around its neighborhood (30) (see Fig. 4). From site-directed mutagenesis (76), low-temperature SA and circular dichroism (77), low-temperature time-resolved fluorescence (29), Chl 627(29) has been assigned as the most probable candidate for the lowest-energy Chl in CP47, although some studies proposed Chl 612(11) or Chl 624(26) (75,78). It is likely that our experimental findings are in a good compliance with the abovementioned assignments (i.e., either Chl 634(43) or Chl 636(45) is the low-energy pigment of CP43 and Chl 627(29) is the lowest-energy pigment of CP47). Because the lowest-energy Chl of CP43 is excitonically coupled with a larger number of Chls, it has been suggested to have larger oscillator strength compared with the one of CP47, which maintains a loose excitonic interaction with the neighboring Chls (30). The observed well-defined F lineshape of the aggregated species in CP43 presented in this study is most likely to result from a conformational rearrangement that induces clustering of the lowest-energy Chls (which themselves have larger oscillator strength) with a number of strongly coupled neighboring Chls. On the other hand, the observed relatively weak F of aggregated species in CP47 is likely to be originated from a conformation rearrangement-clustering of Chls 627 (28) with its loosely coupled neighboring Chls that are available in a small number.

Interestingly, the analyses of the SF spectra of aggregated CP43 and CP47 described in this work could not reveal the presence of a far-red band located around 730-nm wavelength region. This finding suggests that carotenoids (β-carotene) available in the core antenna complexes cannot produce such a far-red band in their aggregated states. It can also be that the aggregation of the core antenna complexes does not confer suitable avenues for enhanced Chl-Car interaction, which would lead to the formation of a such a far-red band. The absence of the far-red band in the aggregated core antenna complexes substantiates well our earlier proposition that the carotenoid lutein 1 in the terminal emitter domain is involved in the formation of the far-red band in the peripheral (major and minor) antenna complexes (34,35). By yielding the far-red emission band upon aggregation, lutein 1 is suggested to form energy-dissipating channels in both major and minor light-harvesting antennas (LHCII, CP24, and CP26) (34,35). Therefore, the absence of far-red emission band in the core antenna aggregates points strongly to the possibility that these complexes (CP43 and CP47) are not involved in Chl-Car *CT* state-associated quenching.

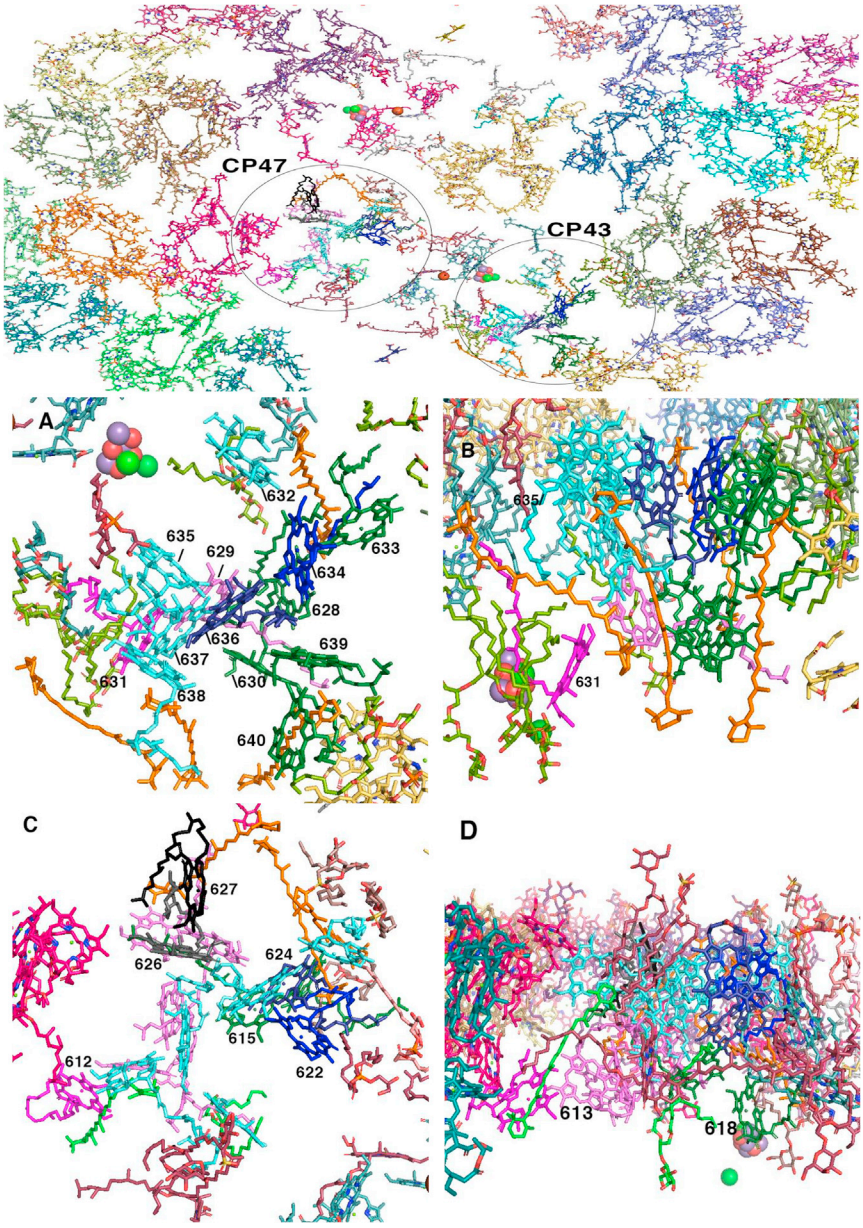

FIGURE 4 Views of pigments from the crystal structure of PSII of *Chlamydomonas reihardtii* (73). Above is the top view from cytoplasm toward the membrane of PSII, showing CP43 and CP47 Chl inside the circles; (*A*) CP43, top view from cytoplasm; (*B*) CP43, side view oriented with the lumen below; the Chls are suggested to have low energy in CP43 are 634(43) in blue, 636(45) in dark blue (other 4 Chl of the exciton domain are in *light blue*) and 631(37) in pink, forming an exciton domain with 629(34) in light pink; (*C*) CP47, top view from cytoplasm; (*D*) CP47, side view, with lumen below; in CP47, suggested low energy level Chls 612(11) are in pink (613, 614, 616, and 617 are in *light pink*), 622(24) is in blue, 624(26) is in dark blue (619, 620, 621, 623 and 625 is in *light blue*), 615(14) and 618(17) are in green, 626(28) is in gray, and 627(29) is in black. Images were generated using Pymol software (structure from Protein Data Bank, PDB: 6KAD). To see this figure in color, go online.

CONCLUSIONS

Stark spectroscopy is a very powerful experimental tool for resolving overlapping spectral species of excitonically coupled photosynthetic pigment-protein complexes and, at the same time, revealing their underlying physical properties and excited-state dynamics. To uncover the nature and physical properties of the produced spectra, SF spectroscopy was applied to the core antenna complexes CP43 and CP47 in their aggregated states obtained via detergent removal. Although the aggregated core antenna complexes resemble apparently similar spectral profiles of peripheral antenna complexes (of higher plants and diatoms) (34–36), the systematic mathematical modeling of the SF spectra with the aid of conventional Liptay formalism revealed that, in terms of the number of spectral constituents, they are different. In contrast to the peripheral antenna complexes, the aggregated state of both core antenna complexes is characterized by a single quenched species featured with noticeably broad and inhomogenously broadened emission lineshape, peaking around the 700-nm region. From the comparison with the results of aggregated peripheral antenna complexes, we attribute the only quenched species of core antenna complexes to originate from the enhanced Chl-Chl interaction due to aggregation. One of the interesting findings of this study is that the broad spectral species around 730 nm present in aggregated peripheral antenna complexes is absent in aggregates of core antenna

complexes. The 730-nm emission species of the aggregated peripheral antenna complexes was attributed to originate from the enhanced Chl-Car (lutein 1) interaction associated with the formation of an energy dissipation channel. Therefore, from the absence of the 730 nm band, it can thus be concluded that conformational change of core antenna complexes after aggregation does not yield enhanced Chl-Car interaction associated with the energy dissipation channel.

SUPPORTING MATERIAL

Supporting material can be found online at https://doi.org/10.1016/j.bpj.2021.02.037.

AUTHOR CONTRIBUTIONS

Md.W., A.M.A., and R.v.G. designed experiments. H.v.R. prepared CP43 and CP47 complexes. A.M.A., C.I., S.D.'H., and Md.W. prepared aggregated samples. Md.W. and A.M.A. carried out Stark experiments. A.M.A., M.K.A., and Md.W. performed Stark data analysis. A.M.A., C.I., S.D.'H, R.v.G., and Md.W. wrote the manuscript.

ACKNOWLEDGMENTS

The authors thankfully acknowledge the contribution of Jos Thieme for his technical assistance.Md.W., A.M.A., C.I., and R.v.G. were supported by the Vrije University Amsterdam, the Laserlab-Europe Consortium and the advanced investigator grant (267333, PHOTPROT) from the European Research Council. Md.W., C.I., and R.v.G. were supported further by the TOP Grant (700.58.305) from the Foundation of Chemical Sciences, part of NWO. C.I. was awarded an EU FP7 Marie Curie Reintegration Grant (ERG 224796).

REFERENCES

1. Dekker, J. P., and E. J. Boekema. 2005. Supramolecular organization of thylakoid membrane proteins in green plants. *Biochim. Biophys. Acta.* 1706:12–39.
2. Liu, Z., H. Yan, …, W. Chang. 2004. Crystal structure of spinach major light-harvesting complex at 2.72 A resolution. *Nature.* 428:287–292.
3. Boehm, M., E. Romero, …, P. J. Nixon. 2011. Investigating the early stages of photosystem II assembly in Synechocystis sp. PCC 6803: isolation of CP47 and CP43 complexes. *J. Biol. Chem.* 286:14812–14819.
4. Umena, Y., K. Kawakami, …, N. Kamiya. 2011. Crystal structure of oxygen-evolving photosystem II at a resolution of 1.9 Å. *Nature.* 473:55–60.
5. Horton, P., and A. Ruban. 2005. Molecular design of the photosystem II light-harvesting antenna: photosynthesis and photoprotection. *J. Exp. Bot.* 56:365–373.
6. van Grondelle, R., J. P. Dekker, …, V. Sundstrom. 1994. Energy transfer and trapping in photosynthesis. *Biochim. Biophys. Acta. Bioenerg.* 1187:1–65.
7. Bricker, T. M., and L. K. Frankel. 2002. The structure and function of CP47 and CP43 in Photosystem II. *Photosynth. Res.* 72:131–146.
8. Zouni, A., H. T. Witt, …, P. Orth. 2001. Crystal structure of photosystem II from Synechococcus elongatus at 3.8 A resolution. *Nature.* 409:739–743.
9. Kamiya, N., and J.-R. Shen. 2003. Crystal structure of oxygen-evolving photosystem II from Thermosynechococcus vulcanus at 3.7-A resolution. *Proc. Natl. Acad. Sci. USA.* 100:98–103.
10. Biesiadka, J., B. Loll, …, A. Zouni. 2004. Crystal structure of cyanobacterial photosystem II at 3.2 Å resolution: a closer look at the Mn-cluster. *Phys. Chem. Chem. Phys.* 6:4733–4736.
11. Loll, B., J. Kern, …, J. Biesiadka. 2005. Towards complete cofactor arrangement in the 3.0 A resolution structure of photosystem II. *Nature.* 438:1040–1044.
12. Bricker, T. M., W. R. Odom, and C. B. Queirolo. 1988. Close association of the 33 kDa extrinsic protein with the apoprotein of CPa1 in photosystem II. *FEBS Lett.* 231:111–117.
13. Petersen, J., J. P. Dekker, …, G. T. Babcock. 1990. EPR characterization of the CP47-D1-D2-cytochrome b-559 complex of photosystem II. *Biochemistry.* 29:3226–3231.
14. Manna, P., and W. Vermaas. 1997. Mutational studies on conserved histidine residues in the chlorophyll-binding protein CP43 of photosystem II. *Eur. J. Biochem.* 247:666–672.
15. Alfonso, M., G. Montoya, …, R. Picorel. 1994. Core antenna complexes, CP43 and CP47, of higher plant photosystem II. Spectral properties, pigment stoichiometry, and amino acid composition. *Biochemistry.* 33:10494–10500.
16. Barber, J., and B. Andersson. 1992. Too much of a good thing: light can be bad for photosynthesis. *Trends Biochem. Sci.* 17:61–66.
17. Krause, G., and E. Weis. 1991. Chlorophyll fluorescence and photosynthesis: the basics. *Annu. Rev. Plant Biol.* 42:313–349.
18. Horton, P., A. V. Ruban, and R. G. Walters. 1996. Regulation of light harvesting in green plants. *Annu. Rev. Plant Physiol. Plant Mol. Biol.* 47:655–684.
19. Kumar, A., A. Prasad, …, P. Pospíšil. 2019. Characterization of protein radicals in Arabidopsis. *Front. Physiol.* 10:958.
20. Ishikawa, Y., E. Nakatani, …, Y. Yamamoto. 1999. Turnover of the aggregates and cross-linked products of the D1 protein generated by acceptor-side photoinhibition of photosystem II. *Biochim. Biophys. Acta.* 1413:147–158.
21. Dall'Osto, L., S. Cazzaniga, …, R. Bassi. 2010. Enhanced photoprotection by protein-bound vs free xanthophyll pools: a comparative analysis of chlorophyll b and xanthophyll biosynthesis mutants. *Mol. Plant.* 3:576–593.
22. de Bianchi, S., M. Ballottari, …, R. Bassi. 2010. Regulation of plant light harvesting by thermal dissipation of excess energy. *Biochem. Soc. Trans.* 38:651–660.
23. Ruban, A. V. 2016. Nonphotochemical chlorophyll fluorescence quenching: mechanism and effectiveness in protecting plants from photodamage. *Plant Physiol.* 170:1903–1916.
24. Ruban, A. V., R. Berera, …, R. van Grondelle. 2007. Identification of a mechanism of photoprotective energy dissipation in higher plants. *Nature.* 450:575–578.
25. Pascal, A. A., Z. Liu, …, A. Ruban. 2005. Molecular basis of photoprotection and control of photosynthetic light-harvesting. *Nature.* 436:134–137.
26. Ruban, A. V., and M. P. Johnson. 2015. Visualizing the dynamic structure of the plant photosynthetic membrane. *Nat. Plants.* 1:15161.
27. Ilioaia, C., M. P. Johnson, …, B. Robert. 2011. Photoprotection in plants involves a change in lutein 1 binding domain in the major light-harvesting complex of photosystem II. *J. Biol. Chem.* 286:27247–27254.
28. Edelman, M., and A. K. Mattoo. 2008. D1-protein dynamics in photosystem II: the lingering enigma. *Photosynth. Res.* 98:609–620.
29. Shibata, Y., S. Nishi, …, T. Renger. 2013. Photosystem II does not possess a simple excitation energy funnel: time-resolved fluorescence spectroscopy meets theory. *J. Am. Chem. Soc.* 135:6903–6914.
30. Raszewski, G., and T. Renger. 2008. Light harvesting in photosystem II core complexes is limited by the transfer to the trap: can the core complex turn into a photoprotective mode? *J. Am. Chem. Soc.* 130:4431–4446.

31. Horton, P., A. V. Ruban, …, A. J. Young. 1991. Control of the light-harvesting function of chloroplast membranes by aggregation of the LHCII chlorophyll-protein complex. *FEBS Lett.* 292:1–4.

32. Ruban, A., D. Rees, …, P. Horton. 1992. Mechanism of ΔpH-dependent dissipation of absorbed excitation energy by photosynthetic membranes. II. The relationship between LHCII aggregation in vitro and qE in isolated thylakoids. *Biochim. Biophys. Acta. Bioenerg.* 1102:39–44.

33. Ruban, A., and P. Horton. 1992. Mechanism of ΔpH-dependent dissipation of absorbed excitation energy by photosynthetic membranes. I. Spectroscopic analysis of isolated light-harvesting complexes. *Biochim. Biophys. Acta. Bioenerg.* 1102:30–38.

34. Wahadoszamen, M., E. Belgio, …, R. van Grondelle. 2016. Identification and characterization of multiple emissive species in aggregated minor antenna complexes. *Biochim. Biophys. Acta.* 1857:1917–1924.

35. Wahadoszamen, M., R. Berera, …, R. van Grondelle. 2012. Identification of two emitting sites in the dissipative state of the major light harvesting antenna. *Phys. Chem. Chem. Phys.* 14:759–766.

36. Wahadoszamen, M., A. Ghazaryan, …, R. Berera. 2014. Stark fluorescence spectroscopy reveals two emitting sites in the dissipative state of FCP antennas. *Biochim. Biophys. Acta.* 1837:193–200.

37. Wahadoszamen, M., S. D'Haene, …, R. Berera. 2015. Identification of common motifs in the regulation of light harvesting: the case of cyanobacteria IsiA. *Biochim. Biophys. Acta.* 1847:486–492.

38. Miloslavina, Y., A. Wehner, …, A. R. Holzwarth. 2008. Far-red fluorescence: a direct spectroscopic marker for LHCII oligomer formation in non-photochemical quenching. *FEBS Lett.* 582:3625–3631.

39. Ruban, A., D. Rees, …, P. Horton. 1991. Long-wavelength chlorophyll species are associated with amplification of high-energy-state excitation quenching in higher plants. *Biochim. Biophys. Acta. Bioenerg.* 1059:355–360.

40. Ghanotakis, D. F., D. M. Demetriou, and C. F. Yocum. 1987. Isolation and characterization of an oxygen-evolving photosystem II reaction center core preparation and a 28 kDa Chl-a-binding protein. *Biochim. Biophys. Acta. Bioenerg.* 891:15–21.

41. Dekker, J. P., N. R. Bowlby, and C. F. Yocum. 1989. Chlorophyll and cytochrome b-559 content of the photochemical reaction center of photosystem II. *FEBS Lett.* 254:150–154.

42. Groot, M.-L., R. N. Frese, …, J. P. Dekker. 1999. Spectroscopic properties of the CP43 core antenna protein of photosystem II. *Biophys. J.* 77:3328–3340.

43. Groot, M.-L., E. J. Peterman, …, R. van Grondelle. 1995. Triplet and fluorescing states of the CP47 antenna complex of photosystem II studied as a function of temperature. *Biophys. J.* 68:281–290.

44. Porra, R., W. Thompson, and P. Kriedemann. 1989. Determination of accurate extinction coefficients and simultaneous for assaying chlorophylls a and b extracted with four different solvents: verification of the concentration of chlorophyll standards by atomic absorption spectroscopy. *Biochim. Biophys. Acta. Bioenerg.* 975:384–394.

45. Gilmore, A. M., and H. Y. Yamamoto. 1991. Resolution of lutein and zeaxanthin using a nonendcapped, lightly carbon-loaded C18 high-performance liquid chromatographic column. *J. Chromatogr. A.* 543:137–145.

46. Wahadoszamen, M., T. P. J. Krüger, …, M. Gwizdala. 2020. Charge transfer states in phycobilisomes. *Biochim. Biophys. Acta. Bioenerg.* 1861:148187.

47. Ara, A. M., M. Shakil Bin Kashem, …, M. Wahadoszamen. 2020. Stark fluorescence spectroscopy on peridinin-chlorophyll-protein complex of dinoflagellate, Amphidinium carterae. *Photosynth. Res.* 143:233–239.

48. Wahadoszamen, M., I. Margalit, …, D. Noy. 2014. The role of charge-transfer states in energy transfer and dissipation within natural and artificial bacteriochlorophyll proteins. *Nat. Commun.* 5:5287.

49. Wahadoszamen, M., T. Hamada, …, N. Ohta. 2007. External electric field effects on absorption, fluorescence, and phosphorescence spectra of diphenylpolyynes in a polymer film. *J. Phys. Chem. A.* 111:9544–9552.

50. Moscatelli, A., K. Livingston, …, L. A. Peteanu. 2010. Electric-field-induced fluorescence quenching in polyfluorene, ladder-type polymers, and MEH-PPV: evidence for field effects on internal conversion rates in the low concentration limit. *J. Phys. Chem. B.* 114:14430–14439.

51. Lockhart, D. J., and S. G. Boxer. 1988. Electric field modulation of the fluorescence from Rhodobacter sphaeroides reaction centers. *Chem. Phys. Lett.* 144:243–250.

52. Walters, K. A., D. A. Gaal, and J. T. Hupp. 2002. Interfacial charge transfer and colloidal semiconductor dye-sensitization: mechanism assessment via Stark emission spectroscopy. *J. Phys. Chem. B.* 106:5139–5142.

53. Wahadoszamen, M., T. Nakabayashi, …, N. Ohta. 2006. External electric field effects on absorption and fluorescence spectra of a fullerene derivative and its mixture with zinc-tetraphenylporphyrin doped in a PMMA film. *J. Phys. Chem. B.* 110:20354–20361.

54. Novoderezhkin, V. I., M. A. Palacios, …, R. Van Grondelle. 2004. Energy-transfer dynamics in the LHCII complex of higher plants: modified redfield approach. *J. Phys. Chem. B.* 108:10363–10375.

55. Bublitz, G. U., and S. G. Boxer. 1997. Stark spectroscopy: applications in chemistry, biology, and materials science. *Annu. Rev. Phys. Chem.* 48:213–242.

56. Novoderezhkin, V. I., R. Croce, and R. van Grondelle. 2018. Dynamics of the mixed exciton and charge-transfer states in light-harvesting complex Lhca4: hierarchical equation approach. *Biochim. Biophys. Acta. Bioenerg.* 1859:655–665.

57. Ramanan, C., M. Ferretti, …, R. van Grondelle. 2017. Evidence for coherent mixing of excited and charge-transfer states in the major plant light-harvesting antenna, LHCII. *Phys. Chem. Chem. Phys.* 19:22877–22886.

58. Kwa, S. L., S. Voulker, …, J. P. Dekker. 1994. Polarized site-selection spectroscopy of chlorophyll a in detergent. *Photochem. Photobiol.* 59:219–228.

59. Wahadoszamen, M., T. Nakabayashi, and N. Ohta. 2004. Electric field effects on photoisomerization process of diphenylpolyenes doped in a polymer film as revealed by a field-induced change in fluorescence spectrum. *Chem. Phys. Lett.* 387:124–129.

60. Booth, P. J., R. H. Templer, …, M. Lorch. 2001. In vitro studies of membrane protein folding. *Crit. Rev. Biochem. Mol. Biol.* 36:501–603.

61. Qu, Y.-G., X.-C. Qin, …, T.-Y. Kuang. 2007. Energy transfer of aromatic amino acids in photosystem 2 core antenna complexes CP43 and CP47. *Photosynthetica.* 45:266–271.

62. Wang, J., J. Shan, …, N. Zhao. 1999. Light-and heat-induced denaturation of Photosystem II core-antenna complexes CP43 and CP47. *J. Photochem. Photobiol. B.* 50:189–196.

63. Qu, Y.-G., Y.-D. Gong, …, T.-Y. Kuang. 2006. Structural characteristics of extra-membrane domains and guanidine hydrochloride-induced denaturation of photosystem 2 core antenna complexes CP43 and CP47. *Photosynthetica.* 44:447–453.

64. Ostroumov, E. E., J. P. Götze, …, A. R. Holzwarth. 2020. Characterization of fluorescent chlorophyll charge-transfer states as intermediates in the excited state quenching of light-harvesting complex II. *Photosynth. Res.* 144:171–193.

65. Zubik, M., R. Luchowski, …, W. I. Gruszecki. 2013. The negative feedback molecular mechanism which regulates excitation level in the plant photosynthetic complex LHCII: towards identification of the energy dissipative state. *Biochim. Biophys. Acta.* 1827:355–364.

66. Krüger, T. P., C. Ilioaia, …, R. van Grondelle. 2014. Disentangling the low-energy states of the major light-harvesting complex of plants and their role in photoprotection. *Biochim. Biophys. Acta.* 1837:1027–1038.

67. Ilioaia, C., M. P. Johnson, …, A. V. Ruban. 2008. Induction of efficient energy dissipation in the isolated light-harvesting complex of Photosystem II in the absence of protein aggregation. *J. Biol. Chem.* 283:29505–29512.

68. Pieper, J., J. Voigt, …, G. J. Small. 1999. Analysis of phonon structure in line-narrowed optical spectra. *Chem. Phys. Lett.* 310:296–302.

69. Krüger, T. P. J., V. I. Novoderezhkin, …, R. van Grondelle. 2010. Fluorescence spectral dynamics of single LHCII trimers. *Biophys. J.* 98:3093–3101.

70. Zigmantas, D., R. G. Hiller, …, T. Polívka. 2004. Effect of a conjugated carbonyl group on the photophysical properties of carotenoids. *Phys. Chem. Chem. Phys.* 6:3009–3016.

71. Van Grondelle, R. 1985. Excitation energy transfer, trapping and annihilation in photosynthetic systems. *Biochim. Biophysica. Acta. Rev. Bioenerg.* 811:147–195.

72. Müh, F., Mel.-A. Madjet, and T. Renger. 2012. Structure-based simulation of linear optical spectra of the CP43 core antenna of photosystem II. *Photosynth. Res.* 111:87–101.

73. Sheng, X., A. Watanabe, …, Z. Liu. 2019. Structural insight into light harvesting for photosystem II in green algae. *Nat. Plants.* 5:1320–1330.

74. Hall, J., T. Renger, …, E. Krausz. 2016. Circularly polarized luminescence spectroscopy reveals low-energy excited states and dynamic localization of vibronic transitions in CP43. *Biochim. Biophys. Acta.* 1857:115–128.

75. Reppert, M., K. Acharya, …, R. Jankowiak. 2010. Lowest electronic states of the CP47 antenna protein complex of photosystem II: simulation of optical spectra and revised structural assignments. *J. Phys. Chem. B.* 114:11884–11898.

76. Shen, G., and W. F. Vermaas. 1994. Chlorophyll in a Synechocystis sp. PCC 6803 mutant without photosystem I and photosystem II core complexes. Evidence for peripheral antenna chlorophylls in cyanobacteria. *J. Biol. Chem.* 269:13904–13910.

77. De Weerd, F. L., M. A. Palacios, …, R. Van Grondelle. 2002. Identifying the lowest electronic states of the chlorophylls in the CP47 core antenna protein of photosystem II. *Biochemistry.* 41:15224–15233.

78. Hall, J., T. Renger, …, E. Krausz. 2016. The lowest-energy chlorophyll of photosystem II is adjacent to the peripheral antenna: emitting states of CP47 assigned via circularly polarized luminescence. *Biochim. Biophys. Acta.* 1857:1580–1593.